Australian Journal of Basic and Applied Sciences, 5(3): 60-68, 2011
ISSN 1991-8178

Predicting Density Distribution in Green Compacts Using Finite Element Simulations

[1]Meftah Hrairi, [2]Hedi Chtourou

[1]Mechanical Engineering Department International Islamic University Malaysia
[2]Department of Technology IPEIS, Sfax University, Tunisia

Abstract: Finite element simulation of the rigid die compaction of metal powders can significantly help designers avoid some of the typical problems they face such as the high density gradients within compacted parts and related cracking. In this paper, the modeling of an axisymmetric flanged part using finite element packages ABAQUS and LS-DYNA has been investigated. A material constitutive model of the Cap type, that allows the use of variable elasticity as well as a density dependent Cap aspect ratio, has been implemented into the finite element code ABAQUS whereas the geological Cap model in its conventional form was implemented in the finite element code LS-DYNA. The effect of density distribution in the part was analyzed through the plastic strain that was generated. The results obtained from the two softwares were compared to the experimental density map and a good agreement has been noted.

Key words: Powder metallurgy, compaction, simulation, finite element method.

INTRODUCTION

Parts produced by powder metallurgy (PM) have become increasingly important due to excellent results with small parts for the automobile industry. The number of steel parts made by PM for vehicles has grown significantly in the last decade, and it is expected for this technology to keep substituting normal production methods. The PM industry has enjoyed the benefits of increased content in light vehicles. PM technology provides total cost savings, unique properties, reliability, special materials and design capabilities, quality, and increased performance. Automotive design engineers have been converting castings, forgings, and stamping into P/M when designing new engines and transmissions. Typical PM components in modern engines and transmissions include main bearing caps, planetary carries, chain sprockets, and gears and pinions, hubs for cooling fans, timing pulleys, and synchronizer rings Goto, (2008).

The basic process of P/M consists of mixing, filling, compacting, sintering, and finishing with secondary operations German, (1984). Mixing or blending the powders normally incorporates an organic substance to act as a lubricant during the next step. This mix is tested to ensure conformity with predetermined standards. Then, the powder mix is loaded into a suitable die or mould and consolidated by the application of pressure into what is referred to as a compact. Compacts must have sufficient strength to permit handling without fracture or crumbling, but are in no way strong enough for any engineering application. The compacts are then sintered, generally in a protective atmosphere, to cause the particles to weld together thus generating the strength required for use. Finally, secondary operations are carried out if necessary.

In any process of powder compaction, the distribution of density is not easy to foresee and the mechanical behavior of the part is dependent on density distribution Cedergren, (2002). Furthermore, in the compaction process of metal powders into rigid dies, one of the most common problems is cracking during either the compaction stage or ejection from the die. Therefore, the finite element (FE) based simulation is considered to be a design tool for powder metallurgy parts, as well as for compaction tooling, as this method allows the prediction of stresses and density distributions of the pressed compact prior to the actual tooling manufacturing activity Cedergren, (2002).

In this work, the compaction boundary value problem is formulated following the virtual work principle and solved by the FE numerical method. For this, the tooling components are assumed to behave as linear elastic bodies, whereas a multi-surface elastic-plastic Cap model is adopted for the simulation of the powder material behavior. Two versions of this model have been investigated. The first one consists of the geological Cap model in its conventional form, as it is implemented in LS-DYNA while the second one, that allows the use of variable elasticity as well as a density dependent Cap aspect ratio, has been implemented into ABAQUS. Friction between powders and tooling components is assumed to follow the Coulomb's model. These

Corresponding Author: Meftah Hrairi, Mechanical Engineering Department International Islamic University Malaysia
Email: meftah@iium.edu.my

simulations, together with an experimentally obtained local density map, illustrate the predictive capabilities of the FE model.

Finite Element Formulation:

The compaction process is considered as quasi-static transformation in which the main unknown is the final spatial distribution of density (r(x)) in the pressed part. Considering the fact that the powder material undergoes very large deformations, the small strains hypothesis cannot be retained. Thus we formulated the problem using the logarithmic finite strain tensor e and the Cauchy tensor s as the stress measure Chtourou, (1995)

During this process, every material point of each component of the global system should satisfy the equilibrium condition governed by the momentum balance law. Since no body forces are present in this quasi-static application, the momentum balance equation is written in a Cartesian coordinate system (x_i, i=1,2,3) as follows:

$$\partial\sigma_{ij} / \partial \mathbf{x}_i = 0 \tag{1}$$

In this equation, $\partial\square/\partial\mathbf{x}_i$ is the spatial derivative of the Cauchy stress tensor s in the direction *i*. Two kinds of boundary conditions may be associated with the equilibrium state of each component. In fact, prescribed displacements may be applied on some sub-regions Su of the boundary S:

$$\mathbf{u} = \hat{\mathbf{u}} \tag{2}$$

whereas on complementary sub-regions Sf, characterized by the normal vector n, prescribed surface forces, resulting from the applied pressures or the interactions with other components may be applied:

$$\sigma.\mathbf{n} = \hat{\mathbf{f}}_s \tag{3}$$

For the solution of this Boundary value problem, a weak form of the equilibrium condition is used Dhatt and Touzot, (1984). This form, also known as the principle of virtual work, is obtained by multiplying the momentum balance equation by a field of virtual displacement u* and integrating over the total volume V:

$$W = \int_V u^*.(\partial\sigma/\partial\mathbf{x})dV = 0 \tag{4}$$

The standard procedure of integration by parts leads to the well-known equation showing the internal and the external parts of the virtual work and incorporating the imposed forces BC:

$$W = W_{\text{int}} - W_{ext} = \int_V (\varepsilon^*.\sigma)dV - \int_{S_f} (u^*.f_s)dS_f = 0 \tag{5}$$

Using the appropriate relation between the displacements and the strains ($\varepsilon = B.u, \varepsilon^* = B.u^*$) and the constitutive equation relating the stresses to the strains ($\sigma = H.\varepsilon$), discussed in the following section, one can write after transformation Dhatt and Touzot, (1984):

$$\int_V ([\mathbf{B}^T\mathbf{HB}]u)dV - \int_{S_f} (f_s)dS_f = 0 \tag{6}$$

where H is the constitutive behavior matrix. In matrix form, (eq. 6) can be written as:

$$R = K(u).u - F \tag{7}$$

R standing for the residual vector:

Since the compaction problem involves material, geometrical, as well as contact nonlinearities, the above virtual work equation is treated incrementally using the updated Lagrangian formulation and linearized in order to be solved by the Newton-Raphson iterative method (Chtourou, *et al.,* 1985; Zabaras and Abul Fazal, 1992).

The main unknown in this linearized incremental problem is the displacement increment. Until convergence is reached, it is iteratively calculated using the tangent stiffness matrix [K^T] and the incremental residual vector

from the previous iteration:

$$\left[K^T\right]^{k-1}\left\{\Delta u\right\}^k=\left\{\Delta R_{n+1}\right\}^k \tag{8}$$

Furthermore, the linearization procedure lead to the decomposition of the global tangent stiffness matrix into a material $\left[K_m^T\right]$, a geometrical $\left[K_g^T\right]$ and a contact $\left[K_l^T\right]$ component (Chtourou, *et al.,* 1985; Zabaras and Abul Fazal, 1992):

$$\left[K^T\right]=\left[K_m^T\right]+\left[K_g^T\right]+\left[K_l^T\right] \tag{9}$$

The linearized problem is then discretized and solved by the widely used FE numerical method (Chtourou, *et al.,* 1985). Linear quadrilateral and triangular axisymmetric elements were used to model the various interacting components, whereas special contact elements Hofstetter *et al.,* (1993) were used to implement the Coulomb frictional contact interfaces.

The geometric and contact force components of the tangent stiffness matrix, as well as the material component relative to the elastic tools are automatically computed by the chosen FE solver, namely ABAQUS. However, for the powder medium, the material contribution is separately calculated at the element's integration points level by the means of a user defined subroutine using the UMAT facility of ABAQUS (Chtourou, *et al.,* 1985; ABAQUS, 1998). This material contribution is issued from the constitutive model calculations and corresponds to the rate of evolution of the stress increment with respect to the strain increment. While, for all the elastic-behavior tooling components, this tensor is exactly equal to the elasticity tensor, it is a more complicated tensor for the case of the powder Cap material model discussed in the next section. The numerical implementation of this material model is performed by the closest point projection algorithm and involves local nonlinear computations (Chtourou, *et al.,* 1985; Hofstetter *et al.,* 1993).

Material Constitutive Relations:

The basis for successful predictions of shape distortions or the tendency to develop cracks during pressing, unloading, or ejection of the part from the die is a reliable constitutive model for describing the mechanical response of the powder. Thus, in this analysis, the Cap material model has proven to be the most suitable material model since it has the ability to control the amount of dilatancy produced under shear loading and to model plastic compaction.

The Cap model was originally developed for geological materials. This model has been used to simulate cold die compaction of metal powders and it has shown flexibility in modeling all compaction stages. This model can also be used to simulate the compaction of powders, starting from the loose state up to very high density levels. The first numerical simulations using the Cap model were based on the algorithm proposed by Sandler and Rubin, (1979). This algorithm was found not to be fully coherent with the principles of plastic consistency and associativity of the flow rule and was later corrected for these limitations Simo, (1988). Hofstetter *et al.,* (1993) then proposed an improved formulation of the Cap model yield functions in order to ensure a better numerical stability of the model. They also derived a consistent expression of the algorithmic elastoplastic tangent moduli. The use of this algorithmic moduli in place of the so-called continuum moduli helps to preserve the quadratic rate of convergence when a Newton-Raphson scheme is used for solving the FE problem Hofstetter *et al.,* (1993).

LS-DYNA material model 25:

As shown in Fig. 1, the Cap model consists of three surfaces in the pressure $\sqrt{J_{2d}}-J_1$ space. Surface f_1 is the failure envelope, f_2 is the Cap surface, and f_3 is the tension cutoff that intersect in a non-smooth manner (Hofstetter *et al.,* 1993; Dimaggio and Sandler, 1971).

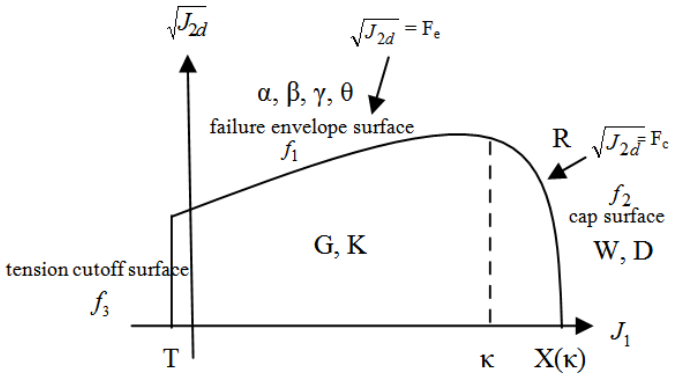

Fig. 1: Yield surfaces of the two-invariant Cap model

The functional form of the failure envelope surface is given by

$$f_1 = \sqrt{J_{2d}} - \min\left(\alpha - \gamma e^{-\beta J_1} + \theta J_1, \left|X(\kappa_n) - L(\kappa_n)\right|\right) \tag{10}$$

where X(κ) and L(κ) are defined by

$$X(\kappa) = \kappa + R(\alpha - \gamma e^{-\beta\kappa} + \theta\kappa)$$

$$L(\kappa) = \begin{cases} \kappa & if\ \kappa > 0 \\ 0 & if\ \kappa \le 0 \end{cases} \tag{11}$$

This failure envelope surface is fixed in $\sqrt{J_{2d}} - J_1$ space, and therefore does not harden unless kinematic hardening is present. The cap surface f_2 is given by

$$f_2 = \sqrt{J_{2d}} - \frac{1}{R}\sqrt{\left[X(\kappa) - L(\kappa)\right]^2 - \left[J_1(\kappa) - L(\kappa)\right]^2} \tag{12}$$

The hardening parameter κ is related to the plastic volume change ε_v^p through the hardening law

$$\varepsilon_v^p = W\left(1 - e^{-D\left(X(\kappa) - X_0\right)}\right) \tag{13}$$

Geometrically, κ is seen in Fig. 1 as the J_1 coordinate of the intersection of the Cap surface and the failure surface. The hardening of the Cap will be modeled through the hardening rule relating the hardening state variable to the volumetric plastic strain in a form suggested by the results of the classical hydrostatic pressing test. Finally, the function f_3 of the tension cutoff surface is given by

$$f_3 = T - J_1 \tag{14}$$

The elastic domain in $\sqrt{J_{2d}} - J_1$ space is then bounded by the failure envelope surface above, the tension cutoff surface on the left, and the cap surface on the right. An additive decomposition of the strain into elastic and plastic parts is assumed:

$$\varepsilon = \varepsilon^e + \varepsilon^p \tag{15}$$

Stress is found from the elastic strain using Hooke's law,

$$\sigma = \mathbf{C}(\varepsilon - \varepsilon^p) \tag{16}$$

where C is the fourth order elasticity tensor.

For the Cap model, and as shown in Fig. 1, a number of parameters must be chosen to represent a particular material. These are generally based on experimental data. The parameters α, β, θ and γ are usually

evaluated by fitting a curve through failure data taken from a set of triaxial compression tests. The parameters W, D, and X_0 define the Cap hardening law. The value W represents the void fraction of the uncompressed sample and D governs the slope of the initial loading curve in hydrostatic compression. The value of R is the ratio of major to minor axes of the quarter ellipse defining the Cap surface. G and K represent the elastic moduli of the material and are expressed as a function of the density.

Cap model Implemented in ABAQUS:

This cap formulation proposed by Hofstetter *et al.* (1993) is somewhat different from the classical ones, proposed by Sandler and Rubin (1979), Simo *et al.* (1988) and Dimaggio and Sandler, (1971), as implemented in LS-DYNA, and offers better algorithmic robustness. It has also been proposed that the aspect ratio R of the cap should be an increasing function of density so as to better represent ductile powder compaction behavior:

$$R(\rho) = \frac{(X(K) - K)}{F_e(K)} \tag{17}$$

Furthermore, the elasticity parameters are density dependent:

$$\mathbf{C} = \frac{\partial^2 \psi}{\partial \varepsilon^2} = 2G(\rho)\mathbf{I} + (K(\rho) - (2/3)G(\rho))\mathbf{1} \otimes \mathbf{1} \tag{18}$$

where I and I are respectively the fourth and second order identity tensors, G and K are the shear and bulk moduli expressed in terms of the powder relative density ρ.

The volumetric plastic strain ε_v^p is the trace of the plastic strain tensor $\boldsymbol{\varepsilon}^{\mathrm{p}}$. It is used to update the actual aggregate density ρ using the initial loose state density ρ_0 as follows:

$$\rho = \rho_0 e^{-\varepsilon_v^p} \tag{19}$$

Furthermore, an associative flow rule was adopted. No experimental observations did in fact justify the use of a more complicated non associative flow rule. The associative flow rule used here for a multi yield surface plasticity is the one defined in equation (15), where $\dot{\lambda}_i$ is the plastic consistency parameter associated with the yield surface function f_i.

$$\dot{\varepsilon}^p = \sum_{i=1,3} \dot{\lambda}_i \frac{\partial f_i(\sigma, K)}{\partial \sigma} \tag{20}$$

The numerical implementation of the constitutive equations presented here requires special care especially when dealing with the singular corners resulting from the non smooth intersection of the yield surfaces. Details on the algorithmic treatment of such a model can be found in Chtourou, *et al.,* (2002)

Numerical Simulation:

In order to illustrate the predictive capabilities of the two cap material models for the compaction of the 316L stainless steel powder, we present the simulation of the compaction process of an industrially produced part. This two-level axisymmetric part is used in a marine motor craft and must exhibit good mechanical properties as well as good corrosion resistance. The initial dimensions of the die cavity, the expected final dimensions of the pressed part, as well as the tooling displacements are given in Fig. 2. The material parameters for 316L stainless steel powder used in these simulations are taken from Chtourou *et al.* (2002).

LS-DYNA simulation:

The initial powder geometry was meshed using solid 168 tetrahedral elements (Fig. 3). In addition, since our main objective was the determination of the compact's density distribution, the simplest and numerically cheapest way to achieve this was to impose nodal displacements at the powder boundary node sets. Therefore the punches were not modeled in this application. The ANSYS™ output file (.k file) is entered into LS-Prepost before changing the parameters' values in accordance to the standard table of units. The LS-Prepost is a valuable tool for ANSYS™ that provides accurate external values rather than solving with ANSYS™ itself. This is done because LS-Prepost has fewer limitations. The analysis is done by the LS-DYNA™ solver which is known to provide accurate results which are key for any complex analysis.

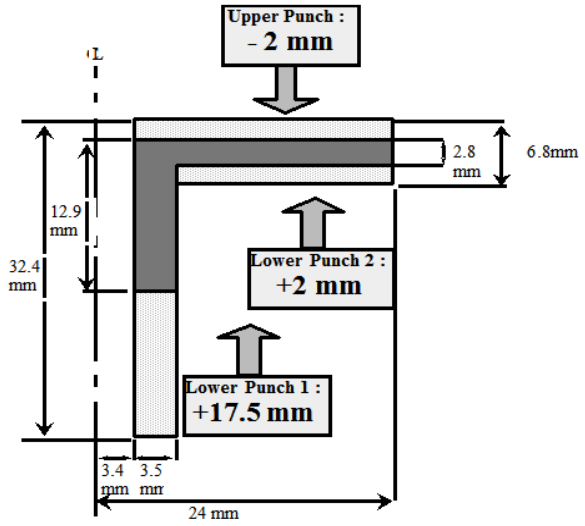

Fig. 2: Axisymmetric two level part before and after compaction

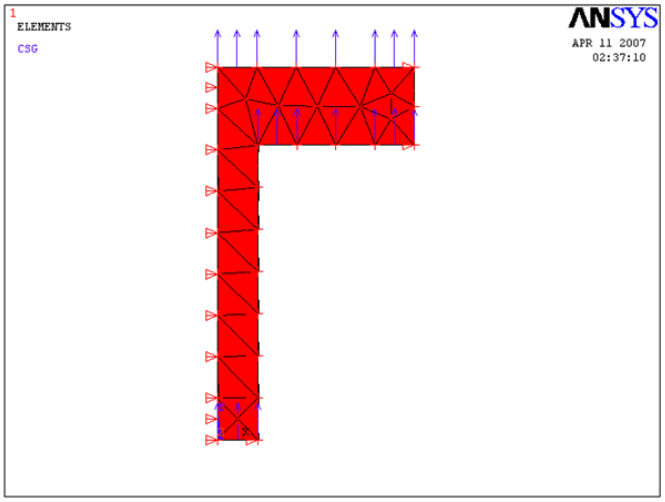

Fig. 3: The flanged part after applying load curve and boundary conditions

ABAQUS simulation:

As shown in the Fig. 4, the initial powder geometry was meshed using three node triangular axisymmetric elements whereas the die and core rod were meshed using quadrilateral four node elements. Similar to the ANSYS simulation, nodal displacements at the powder boundary node sets were imposed and the punches were not modeled. This has very little effect on the density distribution since friction between powder and punches is not as important as in the powder-die or powder-core rod interface. The friction coefficient at these two interfaces was taken to be 0.2.

RESULTS AND DISCUSSIONS

LS-DYNA predicted final densityFrom the simulation, we obtained the displacement and the volumetric plastic strain data that is used to determine the density distribution (Equation 19). Therefore, from the results obtained, calculation of density is done for maximum, intermediate, and minimum values of ε_v^p . The predicted density values will be compared to the density values obtained from an experimental density map as shown in Fig 5. The experimental method for the determination of local density distribution in green

compacts is based on the correlation of Vickers hardness measurements and it has indicated an accuracy of ±1% for densities as high as 86% [14]. From this figure, it can be noted that the density obtained using LS-DYNA™ shows a reasonable agreement with the experimental density map. For example, for the maximum value of density, LS-DYNA™ data shows 89.5% while the experimental data show 87%. Thus, it shows that the bottom part of the flange for LS-DYNA™ experienced the larger loads as it is displaced to 17.5 mm. In brief, the larger the load displacement or the higher the compaction, the higher the density value that results from it.

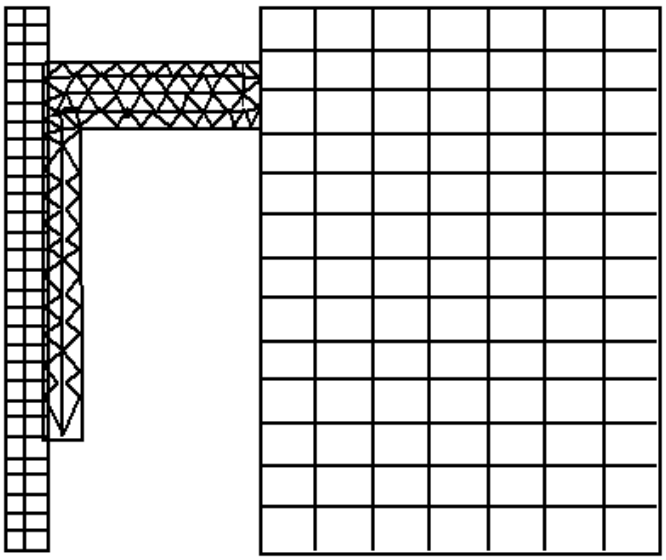

Fig. 4: Initial mesh

On the other hand, for the intermediate density value, LS-DYNA™ data shows 87.7% while the experimental data shows 84%. Nevertheless, for the minimum value of density, LS-DYNA™ data shows 86% while the experimental data shows 81%. In addition, the error percentage for time and displacement obtained are 1.25% and 1.03% respectively. It is a limitation within LS-DYNA™ to have to specify a fixed value of R whereas the latter should be defined as a function of the compact density (Simo, *et al.,* 1988; Dimaggio, and Sandler, 1971; Chtourou *et al.,* 2002).

ABAQUS predicted final density:

The final density distribution predicted by the implemented cap model in ABAQUS via UMAT is displayed on the deformed compact geometry in Fig. 6. It can be noted that the predicted density agrees well with the experimental values of Fig. 5(b) within the experimental method accuracy level of ±1% and within its range of applicability.

ABAQUS FE predicted density map

Finally, due to the part shape, it was suspected that a density gradient could occur in the corner region. This was confirmed by simulation. But as shown in Fig. 5a and 6, this gradient is not very high and thus does not represent a serious crack possibility. Also, it can be noted from these same figures that the predicted final density through the cap model implemented in ABAQUS shows a better agreement with the experimental results when compared to the results obtained by LS-DYNA. This is mainly due to the fact that in ABAQUS, the aspect ratio R is represented by an increasing function of density so as to better simulate ductile powder compaction behavior at each stages. However, in LS-DYNA, R is treated as constant evaluated at the average value of density. As a result, LS-DYNA tends to over predict the density distribution in the powder compaction. Table I depicts the maximum, intermediate and minimum values for the three density distribution maps.

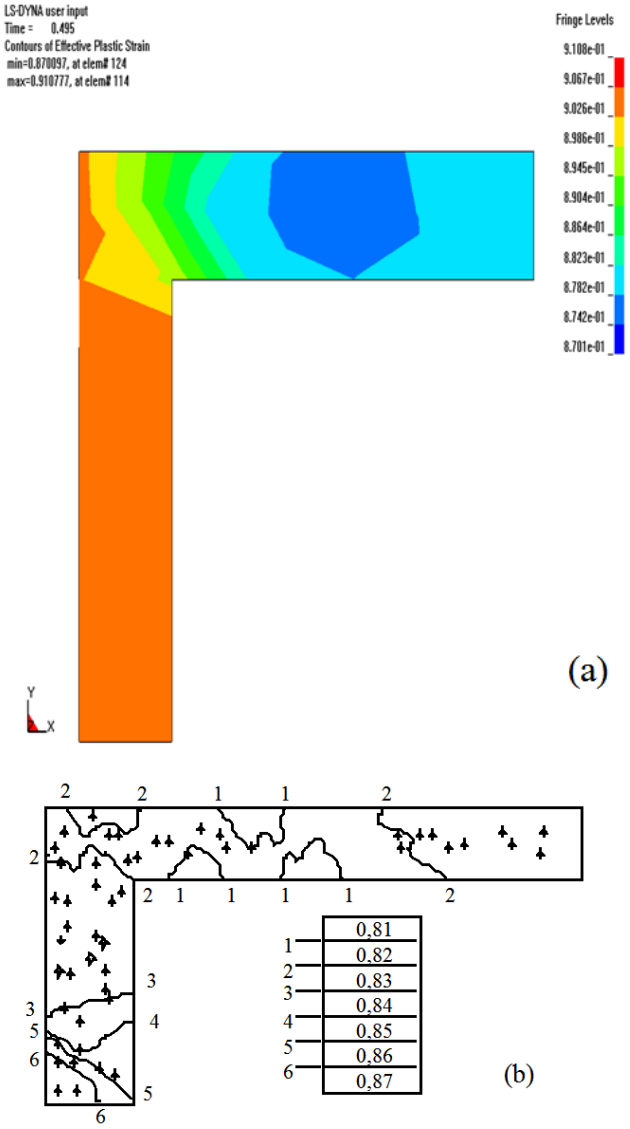

Fig. 5: Map of density distribution a) LS-DYNA™ FE results b) Experimental results

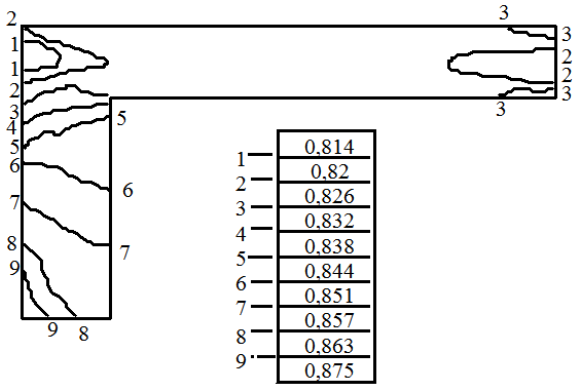

Fig. 6: ABAQUS FE predicted density map

Table 1: Comparison of final density values

	LS-DYNA (%)	ABAQUS (%)	Experimental (%)
Maximum	89.5	87.5	87
Intermediate	87.7	84.4	84
Minimum	86.0	81.4	81

Conclusion:

Numerically, it has been shown that the predicted density distribution using the geological cap model as implemented in FE software LS-DYNA correlate reasonably well with those results obtained experimentally even though it over predicts the final density in the pressed part. This discrepancy is believed to be caused by the fact that the cap aspect ratio R, as well as the elastic moduli, is treated as constant. Consequently, a modified cap model, that allows the use of variable elasticity as well as a density dependent Cap aspect ratio, has been implemented into ABAQUS and the density distribution of the latter showed a good agreement between the experimental results and those obtained using the simulation, with an error margin of approximately 1% corresponding to the precision of the experimental method.

ACKNOWLEDGMENT

The authors would like to thank M. A. Hussin for his assistance in running the LS-DYNA simulation and Lynn Mason for her help in editing this paper.

REFERENCES

ABAQUS, 1998. "Theory Manual", Version 5.8, Hibbit, Karlsson and Sorenson, Inc., Rhode Island.

Cedergren, J., N.J. Sorensen, A. Bermark, 2002. "Three-dimensional analysis of compaction of metal powder," Mechanics of Materials, 34: 43-59.

Chtourou, H., A. Gakwaya, M. Guillot, 2002. "Modeling of the metal powder compaction process using the cap model. Part II: Numerical implementation and practical applications," International Journal of Solids and Structures, 39: 1077–1096.

Chtourou, H., A. Gakwaya, M. Guillot, 2002. "Modeling of the metal powder compaction process using the cap model. Part I: Experimental material characterization and validation," International Journal of Solids and Structures, 39: 1059–1075.

Chtourou, H., A. Gakwaya, M. Guillot, M. Hrairi, 1995 "Implementing a cap material model for the simulation of metal powder compaction," Net Shape Processing of Powder Materials, ASME, AMD- 216: 19-27.

Dhatt, G.S., G. Touzot, 1984. "Une présentation de la méthode des éléments finis," Maloine S.A. éditeur,

Dimaggio, F., I.S. Sandler, 1971. "Material Model for Granular Soils", Journal of the Engineering mechanics Division, pp: 935-950.

German, R.M., 1984. Powder Metallurgy Science. 2nd Edition, MPIF, Princeton N.J.

Goto, R., 2002. "Powder metallurgy growth in the automotive market," Retrieved February 10 2008 http://www.touchbriefings.com/pdf/11/auto031_p_goto.pdf,

Guillot, M., H. Chtourou, S. Parent, 1995. "Local density measurements in green and sintered 316 L stainless steel powder compacts", International Conference on Powder Metallurgy and Particular Materials, Seattle.

Hofstetter, G., J.C. Simo, R.L. Taylor, 1993. "A modified cap model: closest point solution algorithms," Computers and Structures, 46(2): 203-214.

Sandler, I.S., D. Rubin, 1979. "An algorithm and a modular subroutine for the cap model", International Journal for Numerical and Analytical Methods in Geomechanics, 3: 173-186.

Simo, J.C., J.W. Ju, K.S. Pister, R.L. Taylor, 1988. "Assessment of cap model: consistent return algorithms and rate dependent extension", Journal of Engineering Materials, 114-2: 191-218.

Zabaras, N., M.A. Abul Fazal, 1992. "A family of integration algorithms for constitutive equations in finite deformation elasto-viscoplasticity", International journal For Numerical Methods In Engineering, 33: 59-84.